Chapitre 1

Robotic Force Amplification with Free Space Motion Capability

Résumé

Une architecture de commande basée sur l'admittance variable est proposée pour une amplification de force en coopération humain-robot. Cette commande est efficace pour les interactions physiques autant dans l'espace libre que lorsque les mouvements du manipulateur sont contraints. Ceci est possible grâce à une transition active entre les deux modes. La loi de commande variable permet aussi d'annuler les oscillations à hautes fréquences qui peuvent apparaître lors de contacts avec des surfaces rigides. Une analyse mathématique de l'architecture de commande est présentée et une validation expérimental préliminaire pour un banc d'essai à 1 degré de liberté est effectuée.

1.1 Introduction

In recent years, human-robot interaction (HRI) has attracted a great deal of attention in the robotics community, mainly because of the significant potential benefits of an active collaboration between humans and robots (Haddadin et al. [2011], Tsarouchi et al. [2016]). The help of a robotic assistant is indeed highly desirable for precision tasks, heavy load manipulation, rehabilitation and many other tasks. Moreover, the quality and the accessibility of the different interactive sensors allow researchers to develop more effective and intuitive interfaces. The most direct interaction between humans and robots is through physical contact ([De Santis et al., 2008]). In such a situation, the communication is therefore mainly accomplished via the interaction forces.

In industry, this approach has been applied to the assisted manipulation of heavy loads (Akella et al. [1999]). Moreover, some of the assistive devices recently developed can actively interpret the operator's intention to move the payload and make use of static balancing to reduce the required power (Lecours et al. [2012], Mörtl et al. [2012]). This kind of physical human-robot

interaction (pHRI) is also used in exoskeletons, sometimes called body extenders. In this context, the actions are completely commanded by the human operator inside the robotic suit (Kazerooni [1990], Montagner et al. [2007]). A typical solution for unilateral pHRI is to make use of an admittance regulator (Lecours et al. [2012], Ficuciello et al. [2014]). However, if a contact with the environment is required, the dynamics of the system changes and becomes more complex (Eppinger and Seering [1987]). Furthermore, in order to obtain a real assistance from the robot, the force applied by the operator should be augmented at the end-effector. It is therefore desirable to implement a controller that can take into account both free space and constrained situations. An early solution to this problem was formulated in Kosuge et al. [1993] using the concept of Virtual Tool Dynamics. More recently, Lamy et al. [2010] presented a force amplification controller for industrial applications, but emphasized the constrained case.

Currently, the most common application of pHRI is for assistive surgical systems. The interaction can take place through telerobotics (Pitakwatchara et al. [2006]) with a force feedback to a haptic device manipulated by the operator, or through direct contact with the surgical robot (Roy and Whitcomb [2002], Cagneau et al. [2008], Yen and Hung [2013]). An interesting approach is presented in Pitakwatchara et al. [2006] where the master PI controller switches to a simple P controller when the force sensed between the slave and the environment exceeds a certain threshold in order to keep the system stable. Similarly, Yen and Hung [2013] uses adaptive fuzzy logic for the inner position control loop to handle the varying resistive forces of the parallel robot mechanism. The major differences between the medical and the industrial fields are the range of the working space and the force enhancement sensed on the operator side. Indeed, the displacement and the force applied by the surgeon are decreased at the tool for more precision whereas force amplification and large workspaces are required in industrial applications. These differences lead to quite similar control architectures but to different physical issues to be addressed. For instance, if the operator force input is amplified at the end-effector, there is a higher risk of exciting the system into an unstable mode, especially when a high velocity contact occurs with a rigid surface. Industrial cooperation robots must deal with larger workspaces, higher velocities and larger forces, but they still need precision for complex tasks.

In this chapter, an effective force amplification controller based on the admittance model presented in Lecours et al. [2012] is proposed for pHRI industrial applications. The first section of the chapter describes the proposed control architecture. The second section investigates the impact of the different parameters on the dynamics of the system, briefly recalls the free space motion control law (Lecours et al. [2012]), and presents a continuous control law used for mode transition. The third section presents a discontinuous control law that allows the system to cancel undesirable behaviours. The last section provides an experimental demonstration of the controller's effectiveness. Here, the term free space motion refers to the mode in which the robot end-effector is able to move in its free space with the help of a physical interaction, also

known as, unilateral interaction. By contrast, in the constrained mode, the human interaction helps the robot end-effector to rest against a rigid environment and apply a force, also known as, bilateral interaction.

1.2 Control architecture

Cooperative force amplification implies a direct contact between the robot and the human operator, and thus force sensors are required to measure the operator input and the environment output. For simplification purposes, the analysis and the experiments presented in this chapter are developed for a one-degree-of-freedom (dof) robot. Therefore, the system includes only two force sensors, one for the input and one for the output. However, the proposed approach is easily extended to a multi-dof robot using the Jacobian matrix. If the robot is in contact with its environment and no motion is possible, it is easy to implement a direct force control with a certain amplification factor included in the loop (Cagneau et al. [2008]). However, when the system is not constrained by its environment and is required to move freely in its working space, the direct force control becomes inefficient for a precise positioning or for velocity control. Force control alone is thus not an adequate option for a system that must be able to operate in both constrained and free spaces. A possible approach to address the latter issue is admittance control, which allows the transformation of a force into a motion, namely position or velocity (Lecours et al. [2012], Lamy et al. [2010], Yen and Hung [2013]). The admittance is derived from the impedance that captures the relationship between motion and force. These two terms have been loosely used in the literature in the past years, but for the purposes of this thesis impedance represents the transformation of a motion into a force while admittance represents the opposite, as stated previously.

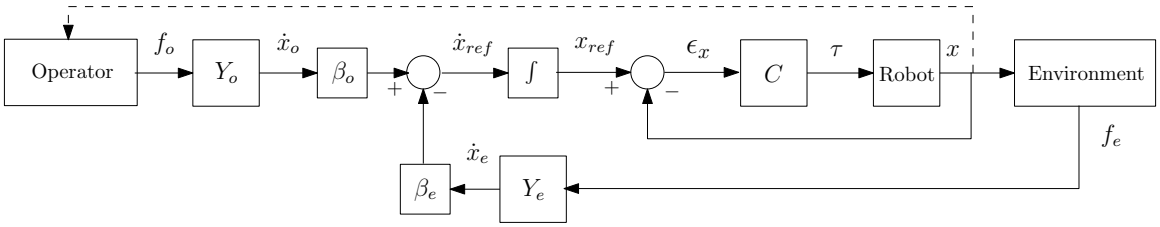

FIGURE 1.1 – Architecture of the enhanced admittance controller for a pHRI force amplification.

Fig. 1.1 presents the architecture proposed for the cooperative force controller. Variables f_o, Y_o, $\dot{x}_o$, and β_o represent respectively the force applied by the operator, the operator admittance relationship, the resulting operator velocity, and the operator amplification factor while f_e, Y_e, $\dot{x}_e$, and β_e are defined similarly for the environment. Variables x_{ref}, x, and ϵ_x are the desired position, the actual position, and the error between these two positions while τ is the torque command to the robot. The controller includes two loops, namely, an inner loop for the precise positioning and an outer loop for the transformation of the different forces interacting with

the robot into desired motions. The components of the controller are explained in more detail in the following subsections.

1.2.1 Inner position control loop

The first basic principle when using admittance control is to include an inner motion control. This controller, represented by C in Fig. 1.1, is used to follow a desired velocity or position. In the context of force amplification, a position control is more intuitive considering the strong relationship between a displacement and a force acting on an object having a certain stiffness (Hooke's law). Furthermore, the possibility to use the same controller for autonomous free space motion is an advantage. Due to the position control, an integral term appears in the closed loop which introduces an additional pole in the system dynamics. Implementing a PID regulator would thereby potentially compromise the stability of the system with a second additional integral, it is therefore wise to choose a PD regulator for the inner controller. Indeed, the derivative action introduces a zero that provides phase lead, and thus tends to stabilize the closed-loop system. The PD control law is written as

$$\tau = k_p(x_{ref} - x) + k_d(\dot{x}_{ref} - \dot{x}) \tag{1.1}$$

where k_p and k_d are respectively the proportional and the derivative gains.

1.2.2 Outer force control loop

The second basic component of an admittance control architecture is the transformation of the input force into a motion command. Typically, the relationship is of the form

$$f = m(\ddot{x} - \ddot{x}_t) + c(\dot{x} - \dot{x}_t) + k(x - x_t) \tag{1.2}$$

where f is the external force, m, c, and k are respectively the virtual inertia, damping and stiffness, $\ddot{x}$, $\dot{x}$, and x are the acceleration, the velocity, and the position, and finally, $\ddot{x}_t$, $\dot{x}_t$, and x_t represent the desired trajectory to be followed. Since the input is coming from a physical interaction, the latter three variables should be set to zero. The virtual stiffness, k, should also be equal to zero in order to obtain a free motion. The relationship is then rewritten as follows

$$f = m\ddot{x} + c\dot{x}. \tag{1.3}$$

It is then easy to solve the above equation for the velocity in the Laplace domain, yielding

$$\dot{X}(s) = \frac{1}{ms + c}F(s) = \frac{\frac{1}{c}}{\frac{m}{c}s + 1}F(s) = Y(s)F(s) \tag{1.4}$$

where $\dot{X}(s)$ and $F(s)$ are respectively the Laplace transforms of $\dot{x}$ and f, $Y(s)$ is the admittance, and s is the Laplace variable.

Since there is a force amplification situation, a feedback from the sensed environment force is necessary. Therefore, an admittance regulator is used for each sensed force, namely, the operator force and the environment force. The outer force control law is then based on the following relationships

$$x_{ref} = \int (\beta_o \dot{x}_o - \beta_e \dot{x}_e) dt, \tag{1.5}$$

$$f_o = m_o \ddot{x}_o + c_o \dot{x}_o \tag{1.6}$$

$$f_e = m_e \ddot{x}_e + c_e \dot{x}_e. \tag{1.7}$$

Equations (1.6) and (1.7) can be rewritten as

$$\dot{x}_o = \frac{f_o - m_o \ddot{x}_o}{c_o}, \tag{1.8}$$

$$\dot{x}_e = \frac{f_e - m_e \ddot{x}_e}{c_e}. \tag{1.9}$$

Moreover, when x_{ref} reaches a steady state, the expression inside the integral of (1.5) is then equal to zero, i.e.,

$$\beta_o \dot{x}_o - \beta_e \dot{x}_e = 0. \tag{1.10}$$

Substituting (1.8) and (1.9) into (1.10), assuming very small (negligible) virtual inertia, and assuming both virtual damping coefficients to be equal to $c_o = c_e = c$ then leads to

$$\frac{\beta_o f_o - \beta_e f_e}{c} = 0 \tag{1.11}$$

which finally yields

$$f_e = \frac{\beta_o}{\beta_e} f_o = \beta f_o. \tag{1.12}$$

Hence, a force amplification factor β is obtained based on the amplification factors β_o and β_e, that are respectively applied to the operator and the environment admittances.

1.3 Controller parameters

1.3.1 Stability limits

Stability is of paramount importance in pHRI. Assessing stability is a difficult problem that generally requires more than simple simulations, mainly because of the difficulty to accurately model human input. Also, a limit cycle, characterized by a constant oscillation around a steady state, is also an unwanted situation that is more difficult to predict than clear divergence. Limit cycles produce vibrations and are mostly encountered in the constrained mode because of the particular system dynamics (Eppinger and Seering [1987]). Indeed, in this situation, the environment stiffness, sensor dynamics, and low-pass filtering alter the stability bandwidth, and the controller becomes thus less tolerant to high frequency inputs. This is a common

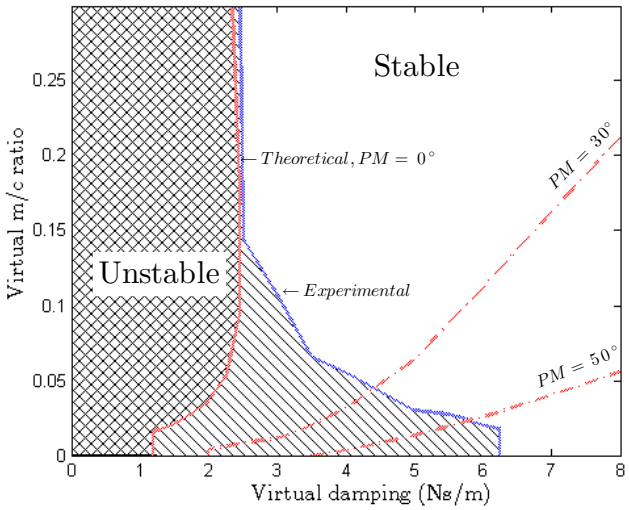

FIGURE 1.2 – Stability limits for the theoretical model and for the experimental setup including the 30° and 50° phase margin limits for the theoretical model.

issue in force control, and it is one major reason to pay a special attention to stability in the constrained mode.

Dynamic linear models of the prototype and the environment described in subsection 1.5.1 have been determined experimentally in order to simulate the robot behaviour. With the constrained system model, the stability limit in terms of the admittance parameters has been estimated and is shown in Fig. 1.2. In this case, Y_o and Y_e are identical, $\beta_o = 1$, and $\beta_e = 1/3$. In simulation, the gain and phase margins on the external open loop have been used to assess the system's stability boundary. The inner loop is already considered as stable, thereby the closed system is defined as stable if the external open loop gain margin is greater than 0dB and the phase margin is greater than 0°. Experimentally, when the system was entering a limit cycle it was not considered stable. The region of instability determined experimentally is larger than the region determined by simulation. This can be explained by two factors. The first one is the imperfect model used in the simulation which also includes model simplifications such as the nonlinearities of the system which were not considered. The second one is the discontinuous contact with the environment when large oscillations occur. It should also be noticed, when looking at the phase margin trend, that, in order to obtain a more robust system, a small m/c ratio is needed. Another parameter that affects the response stability is the amplification factor β_e. In simulation, the system becomes unstable when $\beta_e > 1.7$ while experimentally it becomes unstable when $\beta_e > 0.45$.

In summary, in order to obtain the best performance, the admittance parameters should be as small as possible without crossing the stability limit while β_e, on the other hand, should be as large as possible also without crossing its own stability limit.

1.3.2 Amplification for Low and High Admittances

Continuous control law during free space motion

The first order system defined in (1.4) has a well-known behaviour in the time domain. It is therefore easy to infer the effect of the parameters on the system response for a free space motion situation, namely, the virtual damping defines the response's steady state magnitude while the ratio of the virtual inertia over the virtual damping defines the time required to reach this steady state. The resulting dynamics, when applying an external force, can be considered as that of a mass, m, moving in a viscous environment of damping coefficient, c. Therefore, if the admittance parameters are high then the robot will be less reactive to the sensed force. On the other hand, if they are low it will be easier to move the robot, but more difficult to control it for precise motion. In fact, it has been shown that the most intuitive pHRI can be obtained by varying the admittance parameters online according to the operator's intentions (Lecours et al. [2012], Duchaine and Gosselin [2007], Tsumugiwa et al. [2001]). The approach proposed in (Lecours et al. [2012]) is used here and is now briefly recalled. In this approach, the effective damping coefficient, noted c_{ov}, is calculated based on the nominal (default) damping coefficient, c_o, and the desired acceleration, $\ddot{x}_d$, using

$$c_{ov} = \begin{cases} c_o - \alpha|\ddot{x}_d| & \text{for acceleration} \quad (1.13) \\ c_o + \alpha|\ddot{x}_d| & \text{for deceleration} \quad (1.14) \end{cases}$$

where parameter α is used to adjust the influence of the acceleration, or deceleration, on the variation of c_{ov}. When it is desired to accelerate, the virtual damping decreases and the effective virtual inertia, noted m_{ov}, is also adjusted in order to keep a constant ratio of damping over inertia, which preserves the transient dynamics and makes it easier to move the robot for larger accelerations. However, when it is desired to decelerate, the virtual damping increases, and the virtual inertia partially decreases using an exponential relationship in order to maintain a continuous parameter variation. The following relations are used to adjust the virtual inertia

$$m_{ov} = \begin{cases} \dfrac{m_o c_{ov}}{c_o} & \text{for acceleration} \quad (1.15) \\ \dfrac{m_o c_{ov}}{c_o}(1 - \eta(1 - e^{\gamma(c_o - c_{ov})})) & \text{for deceleration} \quad (1.16) \end{cases}$$

where m_o is the nominal virtual inertia and η and γ are parameters that are used to respectively adjust the steady state inertia to damping ratio and the rate of the transition. In the above, the desired acceleration, $\ddot{x}_d$, is computed using a discrete form of (1.6).

Transition between free space motion and constrained force amplification

As explained in the preceding subsection, in a constrained situation the properties of the environment strongly affect the dynamics of the system. In fact, the stiffness and damping of the contact surface reduce the closed-loop stability bandwidth. On the control architecture side, the feedback admittance can also contribute to instability by acting like a low-pass filter.

The admittance parameters should therefore be chosen carefully. First, both virtual dynamic systems should be identical in order to behave similarly in the process while parameters β_o and β_e take care of the amplification. Moreover, considering Y_o and Y_e as low-pass filters, it becomes obvious that it is not desirable to have one force signal filtered more severely than the other before the subtraction operation is applied. Second, the operator and the environment admittance parameters should be as low as possible while remaining numerically stable. Indeed, lowering these parameters leads to better performances but also reduces the interaction bandwidth, i.e., the robustness. The virtual damping parameters are particularly important because if they are too high the response contains uncontrollable overshoots, due to numerical instability, while if they are too low the stability limit is reached.

A recurrent issue for hybrid position/force control algorithms is the *jittering effect* that appears when the controller is flickering between two states. In the context considered here, the robot should react to two different dynamics, namely, free space and constrained space. In order to obtain the best performances for each case, the controller should take into account these two different modes. The advantage of the admittance control approach proposed here over a hybrid approach is that the behaviour of the controller can be easily modified by a parameter variation without changing the controller architecture (no commutation). Using this feature, it is then possible to define a smooth transition between the free space and constrained motion controls. This transition should allow the robot end-effector to stay on the contact surface when no input force is applied. Moreover, this should not create a *sticking effect* when a rapid pull back from a contact surface is attempted. Hence, the transition control law consists simply in varying the effective damping and inertia parameters. This control law is applied when the external contact force between the robot and the environment, f_e, is comprised between two selected limits noted f_{emin} and f_{emax}. The virtual damping is adjusted according to

$$c_{ov} = c_o - \alpha_{amp}(f_e - f_{emax}) \tag{1.17}$$

where α_{amp} is defined as

$$\alpha_{amp} = \frac{c_o - c_{oamp}}{f_{emax} - f_{emin}} \tag{1.18}$$

in which c_{oamp} is the operator virtual damping for the constrained situation. The virtual inertia is adjusted using

$$m_{ov} = \frac{m_o c_{ov}}{c_o} e^{\gamma_{amp}(c_{ov} - c_o)} \tag{1.19}$$

where γ_{amp} is the smoothness parameter used to adjust the exponential transition. An example is shown in Fig. 1.3 with $f_{emin} = 0.1N$, $f_{emax} = 0.9N$, and $\gamma_{amp} = 3.1$. The virtual damping changes from 8 to $6.5Ns/m$, and the virtual inertia changes from 1 to $0.007kg$.

The dynamics of the force amplification situation can be viewed as two mass-damping systems pushing against one another. When no input force is applied by the operator, the whole system tends to return to its equilibrium, i.e., a zero environment force. If one of the two inertias is

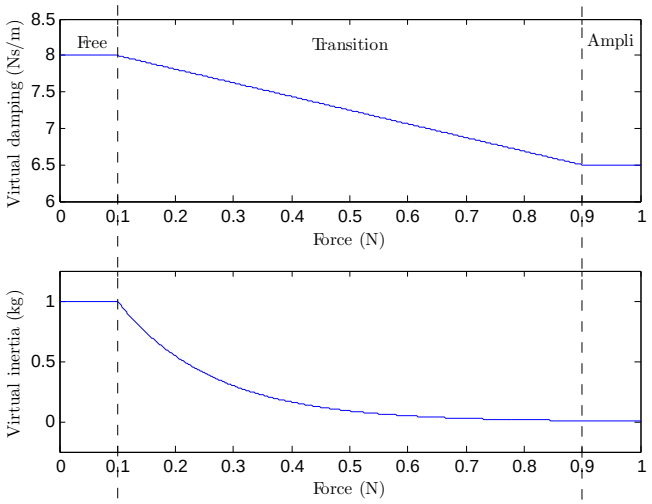

FIGURE 1.3 – Example of the effect of the transition law on the virtual damping and virtual inertia. The force on the x-axis is the contact force measured between the robot and the environment. The admittance parameters transit smoothly from the free space motion mode to the force amplification constrained mode.

larger, or if one of the two damping coefficients is smaller, then the system tends to overshoot on the other side. This explains the need for a smooth increase of the operator admittance parameters when the system approaches the critical zone of zero environment force. It is also understood that if an environment force is sensed, the transition law prevails over the continuous control law, but that if a fast pull back is attempted, the transition law is bypassed because of its small effective range of operation.

1.3.3 Amplification factors

As shown above, in a constrained situation in which Y_o and Y_e have the same admittance parameters as well as small inertias, the force amplification β is solely dependent on β_o and β_e. In this case, one should use both factors to generate the amplification, rather than only one. Indeed, each factor has a significant impact on the system response. Moreover, they represent different specifications due to their location in the force control loop. The first important feature is the change in the feedback steady state gain, given by the variation of β_e, that has a direct incidence on the stability of the system. An increase of this gain positively affects its performance but may also compromise its stability if too high. The second feature is the change in the command steady state gain, given by the variation of β_o, that controls directly the magnitude of the velocity command. Therefore, this parameter complements the first one in order to obtain the desired force amplification β. A variation of β_o has practically no impact on the stability of the system when β_e is chosen appropriately and remains constant. The effect of these factors on the control loop will be demonstrated in the upcoming sections.

1.4 Oscillation canceller

The effect of the different control parameters was established in the preceding section, which led to the development of a stable and fast amplification controller by proper adjustment of the force control loop. However, one issue remains to be addressed in order to make the controller fully reliable, namely the possible occurrence of oscillations for high frequency inputs when admittance parameters are low. A straightforward approach to resolve this issue would be to slightly increase the admittance parameters. Unfortunately, such an approach would slow down the response. Instead, it is proposed here to keep both admittance parameters as low as possible without instability and to actively modify the amplification factors. An appropriate discontinuous variation of the admittance steady state gains through β_o and β_e allows the system to be fast and precise for low to medium frequency inputs, and to cancel oscillations for high frequency inputs. The following algorithm is introduced in order to implement this approach.

$$
\begin{aligned}
\text{If} \quad & (i) \quad f_e > f_{sw} \text{ and } \dot{f}_o > \dot{f}_{osw} \\
& \qquad \text{or} \\
& (ii) \quad \dot{f}_e > \dot{f}_{esw} && (1.20) \\
\text{then} \quad & \beta_e = \beta_c && (1.21) \\
& \beta_o = \beta\beta_e && (1.22) \\
\text{for} \quad & t_i < t \leq t_i + t_c && (1.23)
\end{aligned}
$$

where f_e, $\dot{f}_e$, and $\dot{f}_o$ are respectively the contact force between the robot and the environment, its time derivative, and the time derivative of the force applied by the operator on the input sensor. Also, f_{sw} is the minimum force between the robot and the environment representing a physical contact with an object (contact threshold of the sensor), $\dot{f}_{osw}$ and $\dot{f}_{esw}$ are the maximum time derivatives of the forces for which the system remains stable and has no oscillation and β_c is the minimum environment amplification that leads to a stable response for any input frequency. Finally, t_i is the current time and t_c is the minimum time required to cancel the initiation of an oscillation. Condition (i) limits the output response when the time derivative of the input command exceeds a certain maximum value. It allows the system to remain stable for high frequency command when it is in a constrained situation. Condition (ii) limits the output response when the time derivative of the output exceeds a certain maximum value. It is especially useful for a fast impact situation with a rigid object where f_o is already high and $\dot{f}_o$ does not necessarily vary so much. Equation (1.22) preserves the general amplification relationship.

In other words, the Oscillation Canceller (OC) proposed above allows the process to respond slowly when the time derivative of the force input becomes too large, so as to remain passive with respect to the environment. The force control bandwidth is therefore temporarily

augmented. Furthermore, the OC can be seen as a safe switch that counters fast impulse perturbations or inputs.

1.5 Experimentation

1.5.1 Experimental setup

The novel admittance controller proposed above was validated experimentally using a simple one-dof robot. The experimental setup is shown in Fig. 1.4. It consists of a single revolute joint, a 130mm arm, two single-axis force sensors, and an actuator. One of the force sensors receives the operator input while the other one measures the force generated by the actuator and the operator on the environment. The operator sensor is limited to 5kg and the environment sensor is limited to 20kg. Both sensors are Phidgets Micro Load Cells. The actuator is a Pittman DC Servo Gearmotor with a gearbox ratio of 65.5 :1 and an encoder of 500CPR. The maximum theoretical force that can be generated by the actuator at the end-effector is 26N. The control algorithm is developed with Simulink and RT-LAB. It is then implemented on a real-time QNX computer with a sampling period of 2ms.

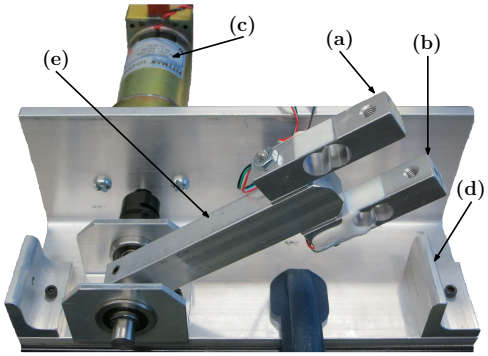

FIGURE 1.4 – One-dof experimental test bench. Components : (a)operator force sensor, (b)environment force sensor, (c)motor, (d)stiff environment, and (e)robot link

Since the effectiveness of the free space motion control law was demonstrated in (Lecours et al. [2012]), the experimental section of this chapter focuses on the constrained situation and the mode transition. Three important properties should be verified in a human-robot force amplification context in order to ensure a natural cooperation, namely : (*i*) the amplification itself, which should be reached at steady-state, (*ii*) the tracking performance so as to achieve the most natural interaction, and (*iii*) the occurrence of vibrations that should be cancelled for efficiency and safety reasons. The performance of the controller proposed in this chapter is demonstrated with the experiments described in the following subsections.

1.5.2 Force amplification for low and high admittances, and high virtual inertia

The first experiment consists in the pursuit of an approximately sinusoidal signal manually generated by an operator with an amplitude of 7.5N, a mean value of 12.5N, and a frequency of approximately 0.4Hz. Three tests were conducted with different sets of parameters in order to assess the tracking performance. The results for a duration of 7.2 seconds are shown in Fig. 1.5. Figure 1.5(a) shows the response with low admittance parameters ($m = 0.007kg$ and $c = 6.5Ns/m$) and an amplification of 4 times the operator input ($\beta_o = 1.6$ and $\beta_e = 0.4$). These admittance parameters are the default ones for a regular operation, and Y_o and Y_e are always similar in constrained mode. Figure 1.5(b) represents a high admittance situation with the same virtual inertia to virtual damping ratio used for the low admittance experiment. As an alternative to directly changing the admittance parameters the amplification factors are reduced while keeping $\beta = 4$ ($\beta_o = 0.8$ and $\beta_e = 0.2$). Reducing the admittance steady-state gains leads to a phase shift of the response. Figure 1.5(c) shows the response obtained with larger virtual inertia values ($m = 0.7kg$ and $c = 6.5Ns/m$) and the default amplification factors. In fact, when the virtual inertia to virtual damping ratio is larger, the response is slower and more overshoots arise.

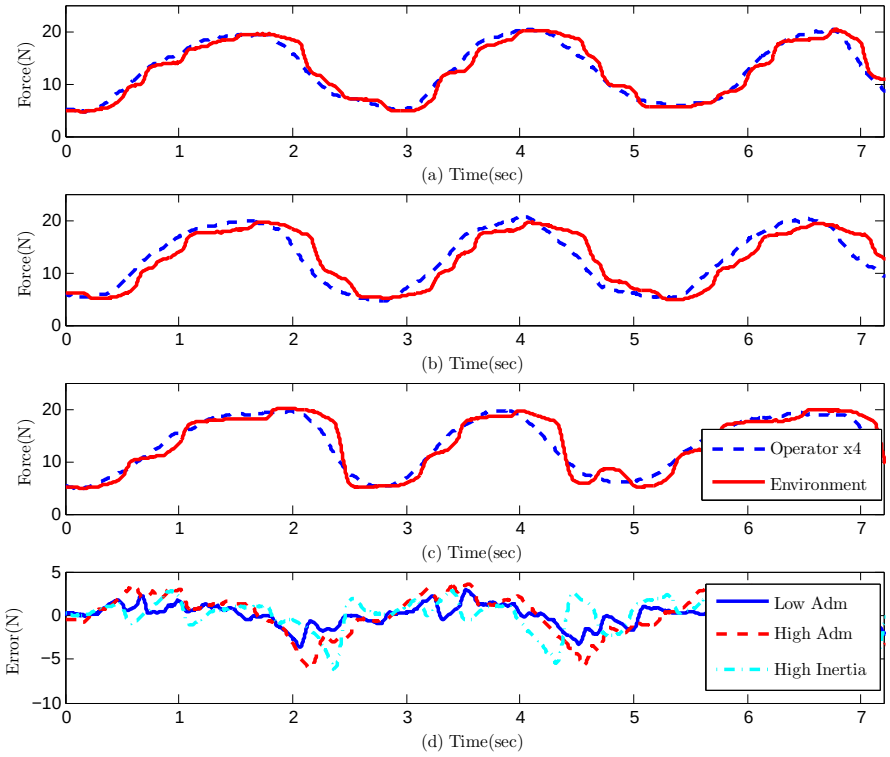

FIGURE 1.5 – (a)Low admittance pursuit, (b)high admittance pursuit, and (c)high virtual inertia pursuit. (d)Error for low and high admittances, and high virtual inertia in the pursuit experiments. The operator force is amplified 4 times on the graphs for comparison purposes.

Figure 1.5(d) shows the error between the operator input and the environment output for each case. The low admittance case seems to give better results than the other two. This is confirmed by the residual sum of squares (RSS), given in Table 1.1, for the 7.2 seconds time period of evaluation. In the experiment reported here, the high virtual inertia performs relatively well, but with the combination of human interaction and overshoots it can become unpredictable, and hence damaging for the response.

TABLE 1.1 – Residual Sum of Squares ($\times 10^4 N^2$)

Low admittance	High admittance	High virtual inertia
0.609	2.038	1.135

1.5.3 Continuous interaction - unconstrained to constrained environment

The second experiment demonstrates how the system behaves for a continuous interaction between the free and the constrained spaces. The interaction consists of a displacement induced by the operator force input, followed by a contact with a stiff environment where the amplification is initiated, then followed by a fast pull back to finally return to a displacement in free space. Figure 1.6 depicts this particular situation with the default admittance parameters. The input (reference) and the response (encoder) velocities of the inner position control loop are shown in Fig. 1.6(a). Velocity plots are shown instead of position plots because they are thought to be more relevant when a physical human interaction feedback is involved. Moreover, the operator force input and the environment force response are represented in Fig. 1.6(b). As expected, it can be observed that an accurate tracking of the reference velocity (resulting of the operator force input) and a zero environment force are obtained in the free space motion mode. On the contrary, and also as expected, an accurate tracking between the operator and the environment forces, and a zero encoder velocity are observed in the constrained mode. In the latter mode, the reference velocity becomes the error between the two amplified admittance outputs, as seen in Fig. 1.1. This error will then reach zero for a steady-state. An interesting behaviour of the controller is shown during the fast pull back (at the end of the force amplification stage). In fact, even if there is no *sticking effect*, as it is observable for the second transition of Fig. 1.6(b), there is a slight phase shift of the encoder velocity due to the high value of the reference velocity when the robot initiates its motion. For a reference velocity below the saturation limits of $\pm 3 rad/s$ the operator should not feel any constraint or inconvenience. The impact of the gearbox backlash is also noticeable on the velocity response when changing directions.

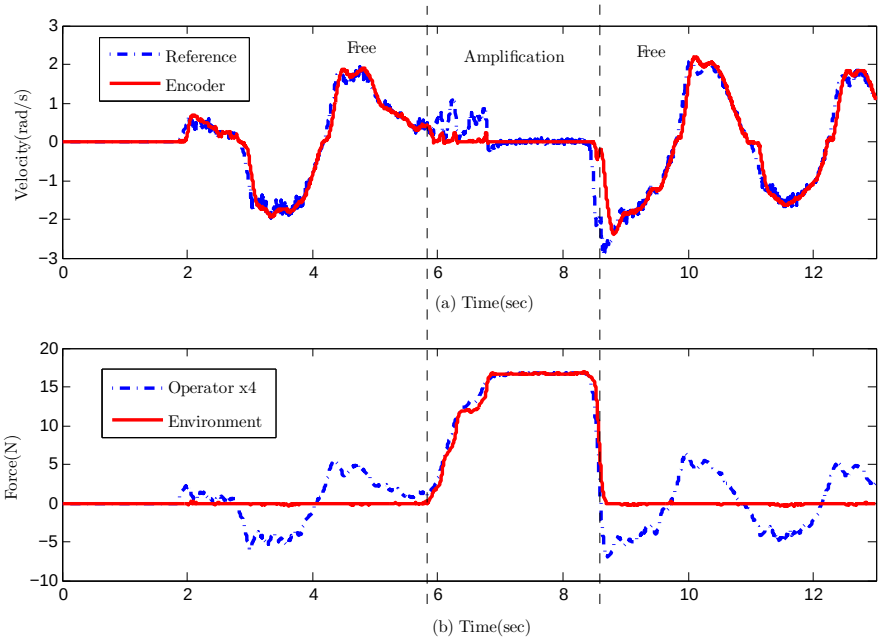

FIGURE 1.6 – Continuous interaction between the free and constrained spaces. (a)Reference and encoder velocities of the robot link, and (b)force sensors signals. The operator force is amplified 4 times for comparison purposes.

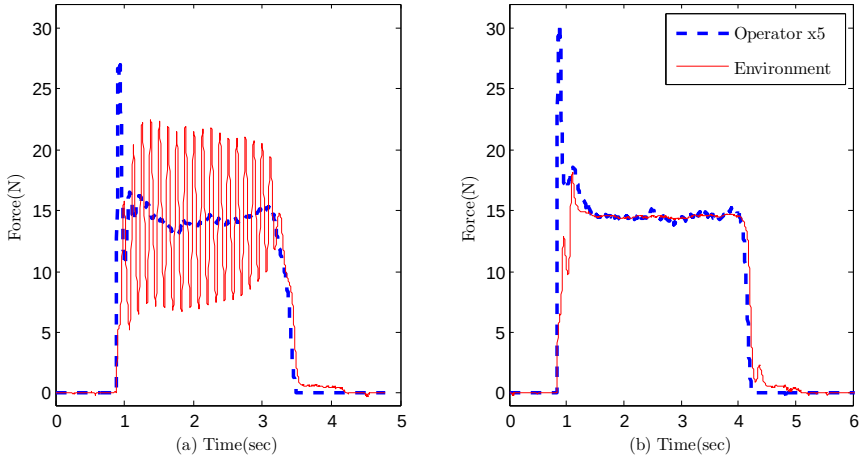

FIGURE 1.7 – Impulse response (a)without the oscillation canceller and (b) with the oscillation canceller. The operator force is amplified 5 times for comparison purposes.

1.5.4 Impulse response - unconstrained to constrained environment

The third experiment reported here is a fast impulse from the unconstrained ($f_e = 0$) to the constrained environment, followed by a constant force input of 3N. In this case, the amplification is 5 times the operator input ($\beta_o = 2$ and $\beta_e = 0.4$). Fig. 1.7 shows two tests, one without the oscillation canceller (a), and one with the oscillation canceller (b). The OC parameters are set to $\beta_c = 0.08$, $t_c = 0.16sec$, $f_{sw} = 0.4N$, $\dot{f}_{osw} = 45Ns/m$ and $\dot{f}_{esw} = 120Ns/m$. With the

OC, all major vibrations or fast impulses are eliminated and the system is therefore able to follow the amplified input. The impact of the transition law is also noticeable in Fig. 1.7. Indeed, when the operator force is released, there is a smooth return to zero of the environment force below $f_{emax} = 0.9N$. As a result, the robot end-effector stays on the contact surface without applying any force.

1.5.5 Video demonstration

The accompanying video demonstrates all situations to be addressed by the controller, namely, free space motion, constrained force amplification and transition between the two (*Chap1_ Force_ Amp_ 1dof.mp4*). The video also illustrates the stability and effectiveness of the controller for fast pull back and sharp contacts (impulses) with a stiff environment. It can be observed that the controller is always stable and that it leads to a very intuitive behaviour. The amplification of the force is also illustrated visually using two identical deformable objects. The video is available at

http://robot.gmc.ulaval.ca/publications/these-de-doctorat

1.6 Conclusion

A novel force amplification controller for pHRI was presented in this chapter. The controller uses the principle of variable admittance in order to optimize the free space and constrained motions. The effect of the different parameters in the force control loop was assessed and explained. Moreover, the experimental results demonstrate that the new approach leads to an intuitive and effective force amplification control, with the help of a smooth transition law and the oscillation canceller. Current work includes the application of the controller to a multi-dof robot.